Ceramics International 51 (2025) 36349–36358

Contents lists available at ScienceDirect

Ceramics International

journal homepage: www.elsevier.com/locate/ceramint

The formation and properties of large-surface-area intergranular mesoporous Al_2O_3 particles

Klara Šparlek [a,b], Romana Cerc Korošec [b], Goran Dražić [c], Anton Meden [b], Erika Švara Fabjan [a,*]

[a] Slovenian National Building and Civil Engineering Institute, Dimičeva ulica 12, 1000, Ljubljana, Slovenia
[b] University of Ljubljana, Faculty of Chemistry and Chemical Technology, Večna pot 113, 1000, Ljubljana, Slovenia
[c] National Institute of Chemistry, Hajdrihova ulica 19, 1000, Ljubljana, Slovenia

ARTICLE INFO

Handling Editor: Dr P. Vincenzini

Keywords:
Mesoporous Al_2O_3
Hydrothermal method
Intergranular porosity
Ethanolamines
Influence of pH
Temperature of thermal treatment

ABSTRACT

Mesoporous γ-Al_2O_3 with pores formed between nanocrystals was synthesized via the hydrothermal method, varying the ethanolamines (monoethanolamine, diethanolamine, triethanolamine), pH values (6.5, 7.5, 8.5) and the temperature of the thermal treatment. Characterization techniques, including nitrogen physisorption, X-ray powder diffraction (XRD), Fourier-transform infrared spectroscopy (FT-IR), thermogravimetric-differential scanning calorimetry-mass spectrometry (TG-DSC-MS), and transmission electron microscopy (TEM), were employed to study the textural and structural properties of the materials. Thermal treatment at 500 °C produced mesoporous γ-Al_2O_3 with pores formed between nanoparticles. The materials synthesized with triethanolamine exhibited the narrowest pore size distribution and the highest specific surface area, particularly at higher pH values. The thermal treatment temperature significantly influenced the textural properties and crystallinity, with γ-Al_2O_3 retained up to 900 °C and the transformation to non-porous α-Al_2O_3 occurring at 1300 °C. These results demonstrate the critical role of synthesis parameters in understanding and optimizing the pore size and phase stability of mesoporous alumina.

1. Introduction

Due to their morphological surface properties and because they exist as different polymorphs, such as γ-Al_2O_3 and α-Al_2O_3, Al_2O_3 materials are interesting materials for application in various fields, including catalysis [1]. Structurally, the polymorph γ-Al_2O_3 is most often considered to be a cubic defect spinel (M_3O_4) [2], while other proposed structures suggest it is a hydrogen spinel (HAl_5O_8) or a non-spinel structure with a monoclinic unit cell. In the literature, γ-Al_2O_3 has often been presented as a material for catalytic support, since it exhibits high thermal stability, a large specific surface area and a uniform framework. Porous materials with pore diameters between 2 nm and 50 nm, considered as mesoporous materials [3], have also been prepared as mesoporous alumina materials [4,5] as well as many other [6,7].

In general, aqueous media synthesis pathways for the preparation of mesoporous alumina suggest using sol-gel [4,5], hydrothermal and precipitation methods, with variations in the precursors and other additives used. For non aqueous syntheses EISA method is often chosen for preparation of mesoporous alumina [8]. Aluminum alkoxide is a frequently used precursor in sol-gel pathways since it allows the properties of materials to be controlled during the synthesis procedure. In water, it hydrolyses and participates as boehmite (γ-AlO(OH) [9]).

Through the preparation of mesoporous alumina using sol-gel, Fulvio et al. [10] studied the influence of precursors on materials' properties. They synthesized materials using the surface active agent Pluronic P123 as the template and boehmite or aluminum isopropoxide as precursors. They found that the pores formed between the nanoparticles and the specific surface was higher when aluminum isopropoxide was used as the precursor, and that the choice of precursor also influences the phase formed. After thermal treatment, the samples synthesized using aluminum isopropoxide were amorphous until 1100 °C, at which point they crystallized to α-Al_2O_3. Conversely, the samples synthesized using boehmite as the precursor consisted of γ-Al_2O_3 after thermal treatment at 400 °C and 600 °C, δ-Al_2O_3 after treatment at 900 °C and δ-Al_2O_3 with θ-Al_2O_3 after thermal treatment at 1100 °C [10]. Sun et al. also used sol-gel synthesis, with $AlCl_3$ as the precursor and a polyethylene glycol

* Corresponding author.
E-mail address: erika.svara-fabjan@zag.si (E. Švara Fabjan).

https://doi.org/10.1016/j.ceramint.2025.05.353
Received 4 April 2025; Received in revised form 12 May 2025; Accepted 24 May 2025
Available online 28 May 2025

PEG. They found that amorphous phase is present up to a thermal treatment temperature of 550 °C and that the transition to the α- Al_2O_3 started at 1300 °C [11]. Teoh et al. [12] and Zhang et al. [13] investigated the effect of pH adjustment during sol-gel synthesis on the phase formed. Teoh et al. synthesized hollow fibers using aluminum isopropoxide and found that after thermal treatment at 300 °C pseudoboehmite fibriles were formed only if the pH value was below 12. The thermal treatment additionally influenced the phase formed. After thermal treatment at 400 °C and 540 °C, the material became amorphous; after treatment at 800 °C, γ-Al_2O_3, θ-Al_2O_3 and δ-Al_2O_3 were formed; and after treatment at 1000 °C and 1050 °C, θ-Al_2O_3, δ-Al_2O_3 and α-Al_2O_3 phases were detected [12]. Zhang et al. used the precipitation method and $NH_4Al(SO_4)_2$ as the precursor. They found that the pores were formed between chains of Al-O. The pH adjustment during synthesis influenced the pore diameter and surface area: with a rise in pH from 8 to 10 during the synthesis, the diameter of the pores lowered, while the specific surface area increased [13]. Fulvio et al. [10], Sun et al. [11], Zhang et al. [13] and Wang et al. [14] all studied the influence of thermal treatment on a material's properties and found that, as the temperature of the thermal treatment rises, the specific surface of mesoporous Al_2O_3 lowers and the pore diameter becomes larger [12–15]. Amirsalari et al. synthesized γ-Al_2O_3 nanoparticles from the precursor $Al(NO_3)_3{\cdot}9H_2O$ and found that a rise in pH from 6 to 10 during the synthesis influenced the size of the crystallites formed. At a higher pH, the crystallites were bigger, while the crystallinity decreased [16]. Additionally, Wang et al. prepared α-Al_2O_3 with isotropic macroporous networks at a pH below pH < 7 and heterogeneous macroporous networks at a pH of 11 [14].

Xu et al., Liu et al. and Gholizadeh et al. all studied the properties of mesoporous alumina prepared via the hydrothermal method [17–19]. Xu et al. found that mesoporous γ-Al_2O_3 with wormhole-like intragranular pores was prepared using glucose as a soft template and $AlCl_3{\cdot}6H_2O$ and $NaAlO_2$ as precursors [17]. Liu et al. reported on the synthesis of mesoporous alumina with $Al(NO_3)_3{\cdot}9H_2O$, which was amorphous up to 600 °C, followed by γ-Al_2O_3 at 800 °C and δ- and α-Al_2O_3 at 1000 °C. They observed that, as the temperature of the thermal treatment increased, the pore size became larger and the specific surface smaller. They also found that changing the base (NH_3, NaOH or Na_2CO_3) in pre-naturalization had an influence on the specific surface and pore size diameter [18].

Wu et al. reported the "pH-adjusting" method for the preparation of the composites Al-SBA-15 and Ti-SBA-15. This method uses precipitation with pH adjustment and hydrothermal treatment. The synthesized material had a high specific surface and narrow pore size distribution at a pH of up to 7.5 and showed a well-defined structure that was lost at a pH of 8.5 [20]. Gholizadeh et al. modified the "pH-adjusting" method to prepare ordered mesoporous alumina and Al_2O_3/Ni catalysts. They used aluminum isopropoxide in an acidic medium and, following the hydrothermal method, the pH was adjusted to a pH of above 7 using ammonia. After the hydrothermal treatment and calcination at 500 °C, they report on the formation of γ-Al_2O_3, showing cubically ordered pore channels, with a pore size of 8.9 nm [19].

Ammonia has very frequently been used as a base for adjusting the pH during the synthesis of mesoporous oxides [12,13,18,20]. However, since it is volatile, adjusting the pH presents a challenging step during the synthesis and reduces the repeatability of the synthesized materials.

The main aim of our work was to investigate, in detail, the properties of mesoporous Al_2O_3 synthesized by a pH-adjusting sol-gel method using different etanolamines, namely etanolamine, diaethanolamine and triethanolamine, followed by hydrothermal treatment. In order to investigate the influence of the thermal treatment on the Al-O phase formed, the crystalline properties of the materials before and after the thermal treatment were investigated. Additionally, the effect of adjusting the pH during the syntheses (pH = 6.5, pH = 7.5 and pH = 8.5), using different ethanolamines (ethanolamine, diethanolamine and triethanolamine), on the morphological and textural properties of the product, as well as on the crystalline phases formed, was investigated in detail using XRD analyses, TG-DSC-MS thermogravimetry, nitrogen sorption, FT-IR spectroscopy and transmission microscopy. To study the thermal behaviour of alumina, the selected materials were thermally treated at different temperatures, namely at 500 °C, 600 °C, 700 °C, 900 °C and 1300 °C.

2. Materials and methods

2.1. Materials

Poly(ethylene glycol)-block-poly(propylene glycol)-block-poly (ethylene glycol) (Pluronic F-127), ethanolamine (MEOA, pH = 14.73, pKa = 9.5, ≥99,0 %), diethanolamine (DEOA, pH = 12,54, pKa = 8,96, ≥99,0 %), triethanolamine (TEOA, pH = 10.60, pKa = 7,76, ≥99,0 %) and aluminum tri-isopropoxide (≥96,0 %) were all purchased from Sigma-Aldrich. Hydrochloric acid (36 %) was purchased from Supelco. Water (for HPLC) was purchased from Honeywell. All chemicals were used without further purification.

2.2. Syntheses

Mesoporous alumina samples were synthesized using the pH-adjusted method with hydrothermal treatment [19]. Different ethanolamines were used to adjust the pH to a variety of values. Firstly, 1 g of Pluronic F-127 was dissolved in a mixture of 50 mL H_2O and 7 mL 36 % HCl in a three-neck 100 mL round-bottomed flask. After mixing for 30 min at 400 rpm (30 × 10 mm magnet) and obtaining a homogenous mixture, the precursor, $Al(O\text{-}i\text{-}Pr)_3$, was slowly added and left to stir at a temperature of 40 °C for another 20 h. After 20 h the mixture had undergone hydrothermal treatment in two 40 mL autoclaves (7/8 fill) at an air temperature of 80 °C for 24 h. In the next step, different ethanolamines (ethanolamine, diethanolamine, triethanolamine) were added to each reaction dropwise until the defined pH was achieved, namely pH values of 6.5, 7.5 and 8.5 (sample labels are presented in Table 1). The start of precipitation could be observed at pH of 3–4. The concentration of bases in the reaction mixtures were 1.2 mmol/L for A-MEOA-6.5, 1.3 mmol/L for A-MEOA-7.5, 1.4 mmol/L for A-MEOA-8.5, 1.2 mmol/L for A-DEOA-6.5, 1.2 mmol/L for A-DEOA-7.5, 1.5 mmol/L for A-DEOA-8.5, 1.7 mmol/L for A-TEOA-6.5, 2.2 mmol/L for A-TEOA-7.5 and 5.0 mmol/L for A-TEOA-8.5. In the next step, the mixture underwent hydrothermal treatment for another 24 h. The autoclave was placed in an air dryer with an air temperature of 80 °C. After 24 h of hydrothermal treatment the precipitant was cooled and filtrated using centrifugation (8500 rpm, 15 min), washed twice with ethanol and dried in an air dryer at 80 °C for 24 h. All samples were kept in a desiccator until the thermal treatment commenced. The temperature program of the thermal treatment was as follows: a heating rate of 1 K/min, followed by 5 h at the defined temperature and a 2 K/min rate cooling down. The defined temperatures were 500 °C, 600 °C, 700 °C, 900 °C and 1300 °C.

2.3. Methods

2.3.1. Nitrogen sorption

Nitrogen adsorption/desorption isotherms were measured at 77 K using an ASAP Micromeritics analyzer. The Brunauer–Emmet–Teller (BET) method was used to calculate the surface area, while the Barrett–Joyner-Halenda (BJH) method with the Kruk-Jaroniec-Sayari (KJS) correction was used to determine the pore size distribution from the adsorption curve. The pore volume was determined using the Gurvich rule. Approximately 80 mg of the sample was analyzed.

2.3.2. X-ray Powder Diffraction Analyses (XRD)

The crystalline phases of the materials were determined using X-ray diffraction (XRD). Measurements were performed on a PANalytical Empyrean X-ray diffractometer with Cu-Kα radiation, at a tube voltage

Table 1
Samples and their labels.

Base	Adjusted pH	Temperature of thermal treatment	Label used for samples	Label used for the group of samples
MEOA	6.5	/	A-MEOA-6.5	A-MEOA
	7.5	/	A-MEOA-7.5	
	8.5	/	A-MEOA-8.5	
	6.5	500	A-MEOA-6.5-500	A-MEOA-500
	7.5	500	A-MEOA-7.5-500	
	8.5	500	A-MEOA-8.5-500	
DEOA	6.5	/	A-DEOA-6.5	A-DEOA
	7.5	/	A-DEOA-7.5	
	8.5	/	A-DEOA-8.5	
	6.5	500	A-DEOA-6.5-500	A-DEOA-500
	7.5	500	A-DEOA-7.5-500	
	8.5	500	A-DEOA-8.5-500	
TEOA	6.5	/	A-TEOA-6.5	A-TEOA
	7.5	/	A-TEOA-7.5	
	8.5	/	A-TEOA-8.5	
	6.5	500	A-TEOA-6.5-500	A-TEOA-500
	7.5	500	A-TEOA-7.5-500	
	8.5	500	A-TEOA-8.5-500	
	7.5	600	A-TEOA-7.5-600	A-TEOA-7.5-T
	7.5	700	A-TEOA-7.5-700	
	7.5	900	A-TEOA-7.5-900	
	7.5	1300	A-TEOA-7.5-1300	

of 45 kV and a tube current of 40 mA. Data was collected in the 2θ range from 10° to 80°, using a 0.007° step and a measurement time of 100 s per step. For low-angle X-ray diffraction, data was collected in a 2θ range from 0.5° to 10°. The results were analyzed using Highscore and Crystallographica Search-Match software. The samples were analyzed before and after the thermal treatment.

2.3.3. Transmission Electron Microscopy (TEM)

The powder samples were examined by conventional and high-resolution transmission electron microscopy (TEM/HRTEM) using a Cs probe-corrected TEM/STEM Jeol ARM 200 CF microscope equipped with a cold-FEG electron source. To minimize the electron-beam-induced damages, an 80 kV accelerating voltage was used. The size of the crystals was determined by averaging the size of 10 crystals from TEM pictures at each temperature of the thermal treatment.

2.3.4. Infrared spectroscopy (FT-IR)

FT-IR spectra were obtained using a PerkinElmer Spectrum 100 FT-IR spectrometer, with the ATR technique and KBr tablets in the range from 4000 cm^{-1} to 400 cm^{-1}. The sample was mixed with the KBr in a weight ratio of 2:118.

2.3.5. Thermal analysis

Simultaneous thermogravimetric and dynamic scanning calorimetry measurements (TGA/DSC) were performed on a Mettler Toledo TGA/DSC1 instrument in the temperature range from 25 °C to 800 °C, with a heating rate of 10 K/min. Approximately 5 mg of the sample was put into 150 μL platinum crucibles, then the furnace was closed and purged for 20 min with air at a flow rate of 50 mL/min to lower the water content in the mass spectrometer. The evolved gases were then transferred to a mass spectrometer (Pfeiffer Vacuum ThermoStar) via the 75 cm heated transfer line. Signals in the range from 1 to 130 m/z were collected. In all measurements a blank curve was subtracted.

In order to study the phase transformation from γ-Al_2O_3 to α-Al_2O_3, some measurements were performed in the temperature range 25–1300 °C. With the exception of the temperature range and the larger initial mass (around 10 mg), all the parameters remained the same.

3. Results and discussion

To study in detail the formation of the synthesized mesoporous Al_2O_3 materials with different ethanolamines – formation of different Al-O phases, by-products, characterization of the materials both before (as synthesized) and after the thermal treatment was performed. The labeling of the samples consists of A for alumina, followed by the labelling of the type of base (MEAO, DEOA and TEOA), adjusted pH (6.5; 7.5 or 8.5) and if applicable, the temperature of the thermal treatment in °C (500, 700, 900 or 1300), as shown in Table 1.

3.1. Properties of the synthesized materials before the thermal treatment

The XRD patterns of all the samples before the thermal treatment are shown in Fig. 1. All the XRD patterns of the A-TEOA samples showed

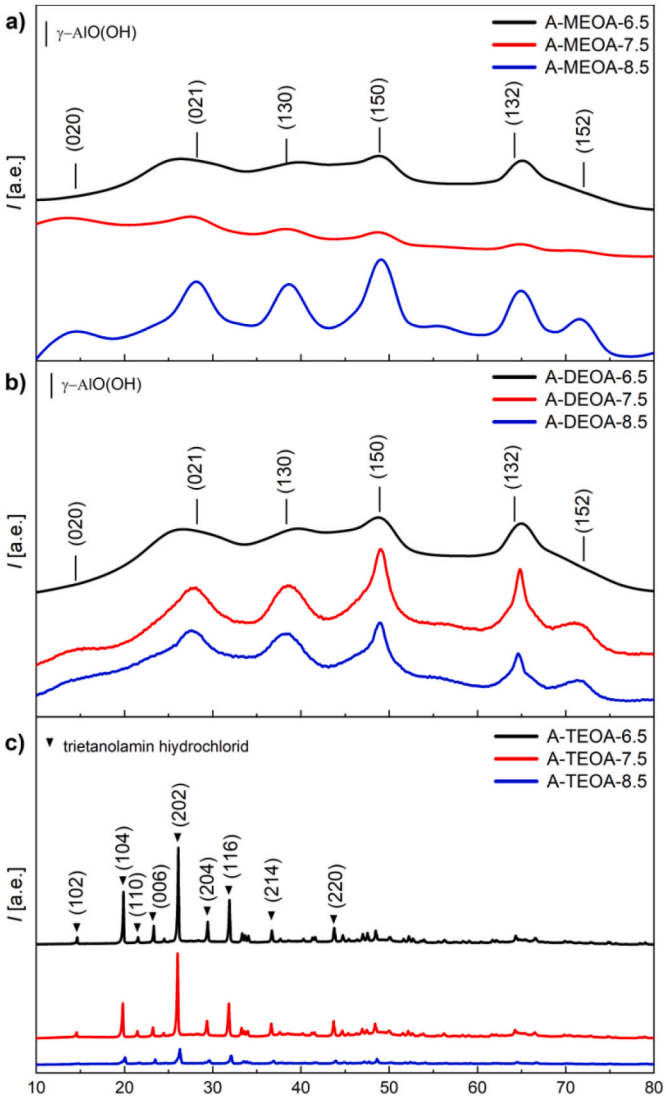

Fig. 1. XRD patterns of a) A-MEOA, b) A-DEOA and c) A-TEOA with crystal planes of γ-AlO(OH) from PDF card 01-073-9093 and triethanolamine hydrochloride from PDF card 00-053-1468.

well-defined strong diffraction peaks at 19.8°, 23.2°, 26.1°, 29.4°, 32.0°, 36.7° and 43.6° 2θ, as well as at many other, lower peaks, indicating a well-crystallized product. It was found that the pattern matches well with that of triethanolamine hydrochloride (PDF card 00-053-1468), which was formed in these samples, and prevented the observation of a low-crystalline Al-O-H phase by XRD.

From the patterns of the samples A-MEOA and A-DEOA, it is clear that these samples have a very low crystallinity, showing broad peaks at about 14.6°, 27.8°, 38.7°, 49.0°, 64.9° and 71.2° 2θ, indicating that structural features, similar to those of boehmite (γ-AlO(OH), PDF card 01-073-9093), started to develop in these samples. The crystallographic order in the samples with the lowest pH during synthesis (A-MEOA-6.5 and A-DEOA-6.5) is so low that the peaks at 14.6° and 71.2° 2θ are not even visible from the amorphous background, yet it can be seen that the peaks become somewhat narrower as the pH during the syntheses increases (samples A-MEOA-8.5 and A-DEOA-8.5), confirming the presence of partly crystalline γ-AlO(OH).

The FTIR spectra of A-MEOA, A-DEOA and A-TEOA are presented in Fig. S1. The FTIR spectra of all the samples showed bands at similar wave numbers, as follows: a broad band at approximately 3280 cm^{-1}, less intensive bands at 2065 cm^{-1} (mostly only confirmed in the A-TEOA samples), a narrow band at 1070 cm^{-1} and less intensive bands at 730 cm^{-1}, 600 cm^{-1} and 450 cm^{-1}. The broad band at approximately 3280 cm^{-1} can be assigned to the ν_{as}(Al)O-H stretching vibrations of γ-AlO(OH), and symmetric and asymmetric bending modes of (Al)O-H groups observed at 1071–1066 cm^{-1}[16,21]. The bands at approximately 630 cm^{-1} were assigned to the stretching modes of octahedral coordination of (AlO_6), the band at 485 cm^{-1} to the bending modes of (AlO_6) in the γ-AlO(OH) [16,21]. Since the vibrations assigned to the vibration typical for γ-AlO(OH) are present in the FTIR spectra of all the samples – also in A-TEOA – we propose that γ-AlO(OH) was formed in all of the samples.

A comparison of the TG and DSC curves for the samples A-MEOA-7.5, A-DEOA-7.5 and A-TEOA-7.5 is shown in Fig. 2. Between room temperature and 100 °C, the samples lose about 2–3 % of the initial mass, which corresponds to the dehydration of the loosely bound physisorbed water, exhibited as an endothermic process on the DSC curves. A closer look at the TG–MS curves (see Supplementary Figures S2, S3 and S4) reveals a slight increase in the 18 m/z signal in this temperature range, which is typical for the evolution of water molecules. The mass of the samples decreases continuously; there is no clear plateau between the dehydration and the further thermal decomposition, which starts at a higher rate, at about 200 °C. On the DSC curves, the beginning of thermal decomposition is revealed as an endothermic process, which, at around 250 °C, turns to an exothermic process. The thermal decomposition of the samples A-MEOA-7.5 and A-DEOA-7.5 is similar. In the temperature range from 100 °C to 800 °C, the mass loss is 39.2 % for the first sample and 46.0 % for the latter. A broad exothermic signal on the DSC curve of the A-MEOA-7.5 sample shows that the main peak is positioned at 300 °C, upon which a small peak at 380 °C is superposed. In the case of A-DEOA-7.5, an additional peak arises at 530 °C, indicating that the decomposition occurs in several successive steps which overlap. From the TG–MS curves we can see that chloride species are evolved at a temperature of 150 °C (35 m/z), most likely in the form of HCl. At around 300 °C, water and carbon dioxide (40 m/z) begin to evolve together, indicating the beginning of thermal decomposition of the organic matter. A typical signal for ethanolamine (30 m/z) is observed, with a slight delay (see Supplementary Fig. S2) [22]. The TG–MS curves of the sample A-DEOA-7.5 are shown in Fig. S3. Another signal, 56 m/z, appeared in the temperature range 250–400 °C, corresponding to the diethanolamine fragment. Since the boiling point of this base is 270 °C, the onset of this signal could be related to its vaporization. The other typical signal for all amines (30 m/z) is more pronounced in the last decomposition range, at 450–650 °C. The highest mass loss, in the 100–800 °C range, shows a TG curve of A-TEOA -7.5, i.e. 58.4 %. The reason for this lies in the fact that TEOA, with a pK_a value of 7.76, is the weakest base among the ethanolamines used in this research work, which is why a higher amount was required to achieve the defined pH value for the A-TEOA samples. The higher percentage of organic phase is consistent with the higher mass loss determined in the TG measurements, so the order of Dm (A-MEOA-7.5) < Dm (A-DEOA-7.5) < Dm (A-TEOA-7.5) is logical. The third exothermic peak of this sample, at 510 °C, is also intense, which could indicate that the decomposition of the amines predominantly takes place in the last step and also coincides with the 30 m/z signal (Supplementary Fig. S4). On the DSC curve of this sample, a sharp endothermic peak with an onset temperature of 168 °C corresponds to the melting temperature of triethanolamine hydrochloride [23]. According to the XRD patterns (Fig. 1) and FT-IR spectra (Fig. S1), the phase formed in the A-MEOA-7.5 and A-DEOA-7.5 samples was γ-AlO(OH), while triethanolamine hydrochloride was also formed in the A-TEOA-7.5 sample. Abdelkader et al. reported an endothermic peak at 380 °C, which corresponds to the dehydroxylation of AlO(OH) to Al_2O_3 [24]. However, the mentioned endothermic peak could not be observed in the DSC curves of our samples, which is probably due to the fact that the thermal decomposition of the organic phase (Pluronic F-127 and amines) overlaps with the dehydroxylation process.

For clarity, in Fig. 3 the DSC curves of the samples A-TEOA-7.5, A-MEOA-7.5 and A-DEOA-7.5 are presented in the temperature range

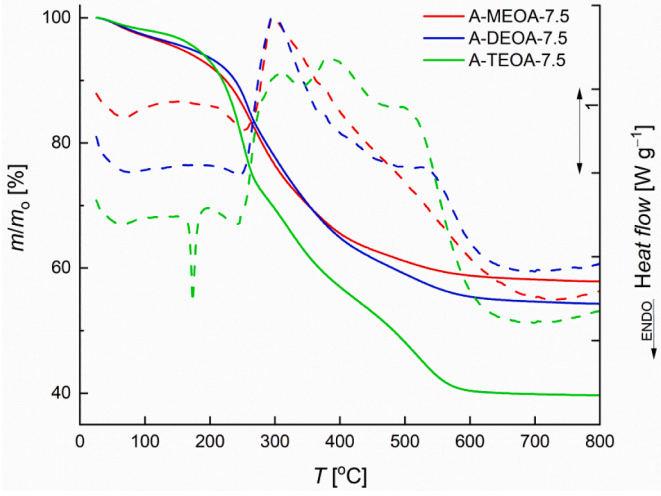

Fig. 2. Comparison of the TG and DSC curves for the samples A-MEOA-7.5, A-DEOA-7.5 and A-TEOA-7.5.

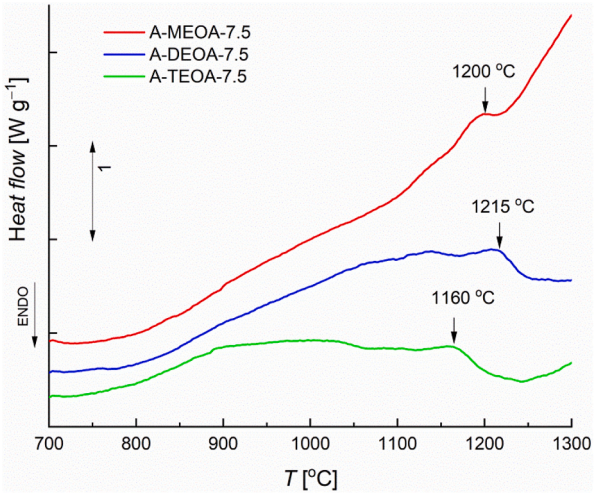

Fig. 3. Comparison of the DSC curves for the samples A-MEOA-7.5, A-DEOA-7.5 and A-TEOA-7.5 in the temperature range 700–1300 °C.

between 700 °C and 1300 °C. From approximately 650 °C, the mass of the samples stayed constant, whereas the signal on the DSC curves turned towards an exothermic direction in all cases. According to Wang et al. [14], the crystallization process of γ-Al_2O_3 takes place in this temperature range, while the exothermic peaks around 1200 °C correspond to the phase transition to α-Al_2O_3 [25]. The phase transformation takes place at the lowest temperature in the sample A-TEOA-7.5 (1160 °C) and at the highest temperatures (1215 °C) in the sample A-DEOA-7.5, indicating that the temperature at which the phase transition occurs depends on the base used in the synthesis.

3.2. Properties of the materials synthesized at different pH values after thermal treatment at 500 °C

The XRD patterns of the samples A-MEOA-500, A-DEOA-500, A-TEOA-500 are shown in Fig. 4. These samples also have a very low crystallinity. However, the broad peaks indicating the onset of crystallographic ordering appear at different positions compared to the samples before thermal treatment. Broad peaks at about 19.8°, 31.8°, 37.3°, 39.6°, 45.9°, 60.6° and 66.7° 2θ can be identified in the patterns of the samples, which is consistent with the spinel-type γ-Al_2O_3 (PDF card 01-079-1558).

It can be seen in Fig. 4 that the lowest peaks at 19.8° and 60.6° 2θ are almost or even completely invisible in the patterns of the samples A-MEOA-6.5-500, A-DEOA-6.5-500, A-TEOA-6.5-500, A-MEOA-7.5-500 and A-DEOA-7.5-500. The samples A-MEOA-8.5-500, A-DEOA-8.5-500 and A-TEOA-8.5-500, synthesized at the highest pH but thermally treated under the same conditions as the others, show significantly better (but still very low) crystallinity. This leads to the conclusion that the slightly better crystallographic order of boehmite (γ-AlO(OH)),

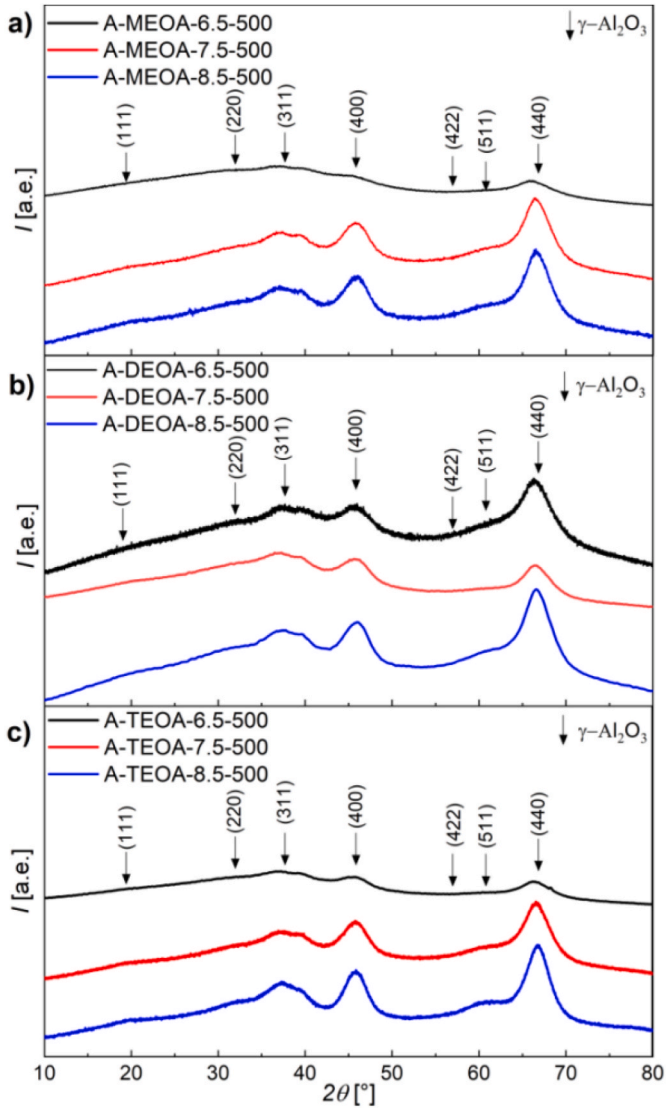

Fig. 4. XRD patterns of the a) A-MEOA-500, b) A-DEOA-500 and c) A-TEOA-500 samples for the crystal planes of γ-Al_2O_3 (PDF card 01-079-1558).

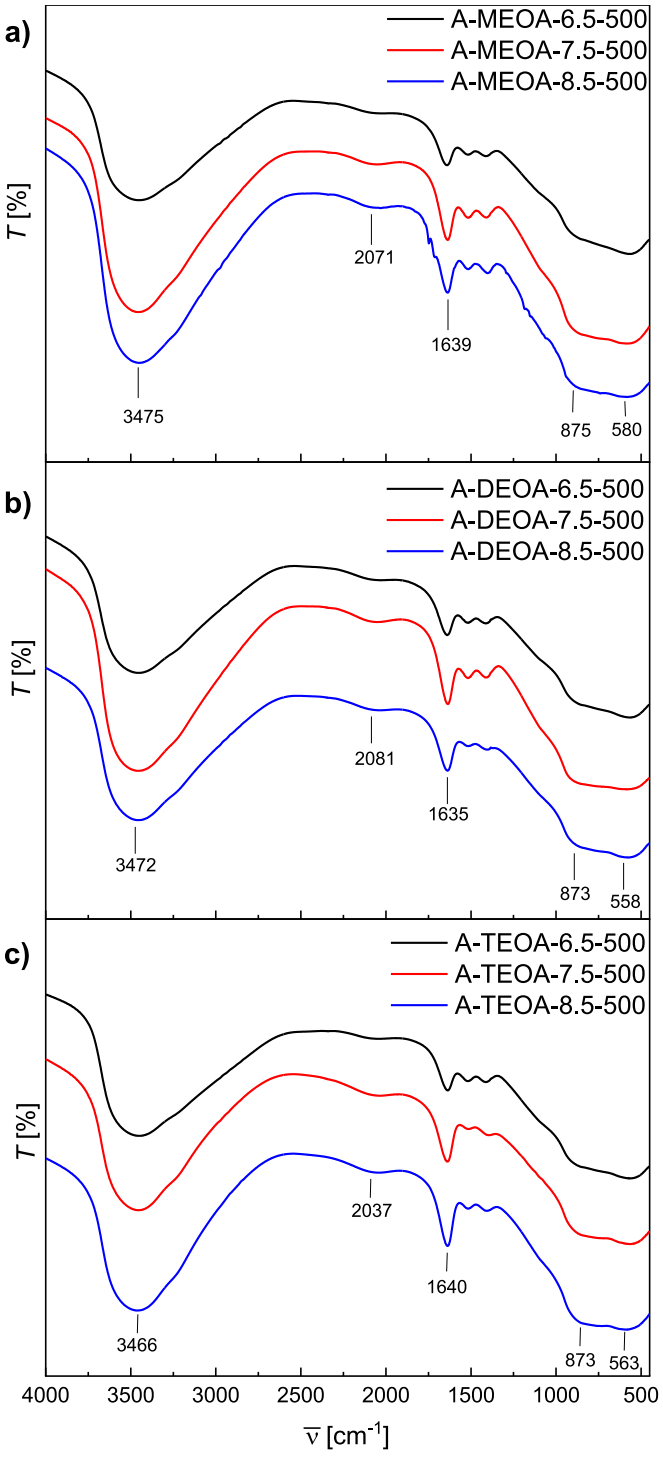

Fig. 5. FTIR spectra of the a) A-MEOA-500, b) A-DEOA-500 and c) A-TEOA-500 samples.

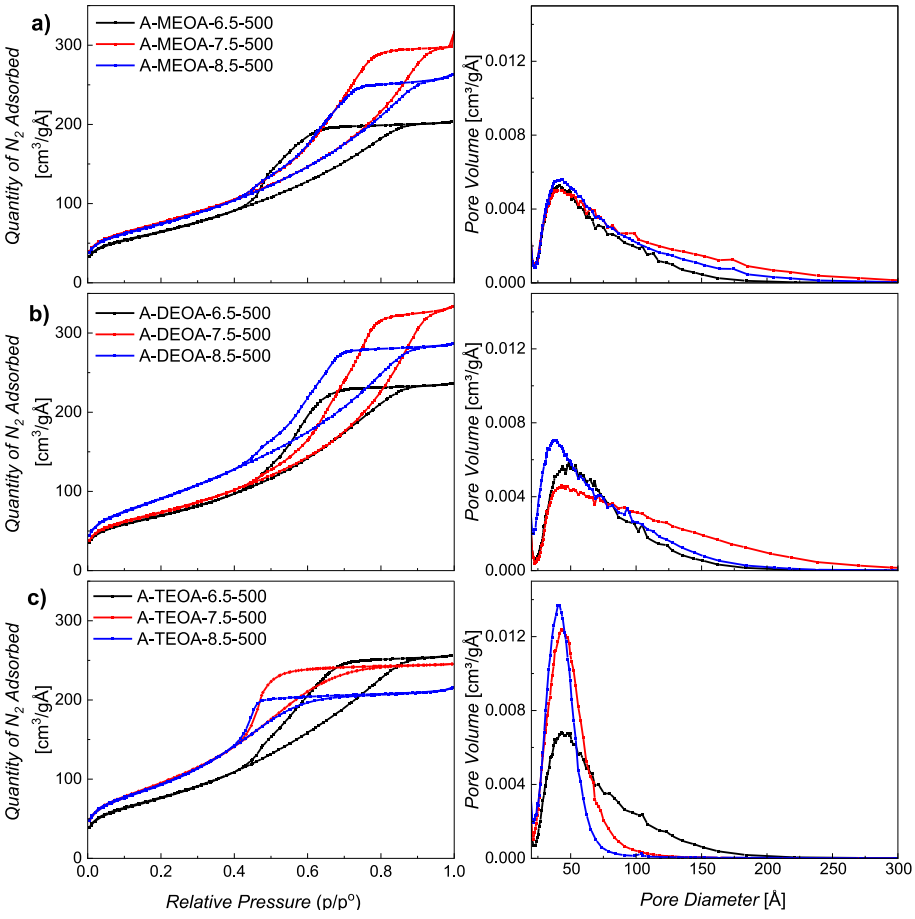

Fig. 6. Nitrogen adsorption–desorption isotherms (left) and BJH pore size distribution (right) of the a) A-MEOA-500, b) A-DEOA-500 and c) A-TEOA-500 samples.

induced by a higher synthesis pH, is transferred to the resulting γ-Al_2O_3 formed during thermal treatment at 500 °C. Amirsalari et al. reported on the preparation of γ-Al_2O_3 nanoparticles from different precursor, Al$(NO_3)_3{\cdot}9H_2O$, and found that the pH influences the crystallinity of the final product, gaining crystalline samples only when the pH during synthesis was higher than 8. They suggested that this is the consequence of increasing NH_4OH, bringing particles closer together and reducing the nucleation [16].

The FTIR spectra of the samples A-MEOA-500, A-DEOA-500 and A-TEOA-500 are presented in Fig. 5. The FTIR spectra of all the samples show bands at similar wave numbers: broad bands at 3470 cm^{-1} and 2070 cm^{-1}, a narrower band at approximately 1640 cm^{-1} and two additional broad bands at approximately 873 cm^{-1} and 563 cm^{-1}. We propose that the band at approximately 3500 cm^{-1} belongs to the stretching vibrations of the OH groups and the band at 1640 cm^{-1} could belong to the bending vibrations of water [16]. Additionally, we propose that the peaks at 563 cm^{-1} and 873 cm^{-1} belong to Al-O vibrations, namely 563 cm^{-1} to bending vibrations and 873 cm^{-1} to stretching vibrations of the Al-O bond [12]. We propose that the broad bands at 563 cm^{-1} and 873 cm^{-1} correspond to Al_2O_3. We have observed that the bands were broader after γ-AlO(OH) transformed to Al_2O_3, as was also reported by Teoh et al. [12]. We observed an absence of the band around 1060 cm^{-1}, which belongs to γ-AlO(OH), and this was present in all the samples before the thermal treatment (Fig. S1). We propose that AlO(OH) was transformed to Al_2O_3, which would also fit the wide bands at 563 cm^{-1} and 873 cm^{-1}.

Table 2
Specific surface, pore volume and pore diameter of the A-MEOA-500, A-DEOA-500 and A-TEOA-500 samples.

Sample name	S_{BET} (m^2/g)	V_p (cm^3/g)	D_p (nm)
A-MEOA-6.5-500	237	0.31	4.2
A-MEOA-7.5-500	279	0.46	4.3
A-MEOA-8.5-500	272	0.40	4.3
A-DEOA-6.5-500	253	0.36	5.3
A-DEOA-7.5-500	268	0.51	4.8
A-DEOA-8.5-500	338	0.44	3.8
A-TEOA-6.5-500	282	0.39	4.6
A-TEOA-7.5-500	302	0.36	4.4
A-TEOA-8.5-500	344	0.33	4.1

The results from the nitrogen physisorption are presented in Fig. 6 and Table 2. The nitrogen adsorption–desorption isotherms and BJH pore size distribution curves of the A-TEOA-500 samples are presented in Fig. 6. Isotherms of all the samples (Fig. 6) correspond to type IV isotherms [3]. We confirmed that all the synthesized samples were mesoporous. The pore size distributions for the A-MEOA-500 (Fig. 6a) and A-DEOA-500 samples are wide (Fig. 6b) and similar for the two groups of samples. Therefore, we propose that adjusting the pH during the synthesis did not affect the pore size distribution of the synthesized materials. It could be observed that the A-TEOA-500 samples possessed the narrowest pore size distribution among the samples (Fig. 6c). Consequently, we propose that, of all the properties of the material, the

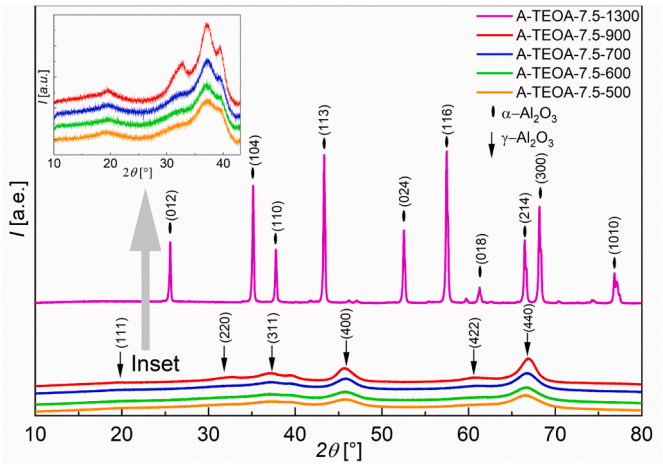

Fig. 7. XRD patterns with inset in the low angle part of the A-TEOA-7.5-T samples treated at different temperatures, with crystal planes of γ-Al_2O_3 (PDF card 01-079-1558) and α-Al_2O_3 (PDF card 01-075-1862).

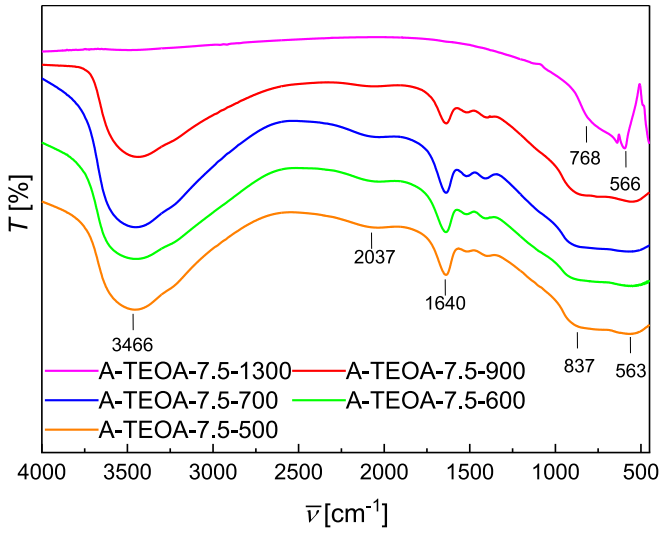

Fig. 8. FTIR spectra of the A-TEOA-7.5-T samples.

base used had the highest impact on the pore size distribution (Fig. 6). The specific surfaces, pore volume and pore diameter of the samples are presented in Table 2.

The pH adjustment and choice of base used during the syntheses affected the specific surface, pore volume and pore size of the A-MEOA-500, A-DEOA-500 and A-TEOA-500 samples differently (Table 2). The most significant effect of the choice of ethanolamine used during the synthesis was observed on the specific surface area of the samples. The S_{BET} of most of the samples increased with the rise in pH, which was adjusted during the synthesis (from 237 m^2/g to 272 m^2/g for the A-MEOA-500 samples; from 253 m^2/g to 338 m^2/g for the A-DEOA-500 samples; and from 282 m^2/g to 344 m^2/g for the A-TEOA-500 samples). However, the effect of adjusting the pH during the syntheses on the pore volume of the materials is not significant, varying between approximately 0.3 and 0.5 cm^3/g. Fulvio et al. [10], with lower specific surface area (235 m^2/g), also reported a broader pore distribution (~5 nm), while the samples in this study— especially A-MEOA-500 and A-TEOA-500— exhibited narrower pore ranges of around 4 nm. Similarly, adjusting the pH value during synthesis did not generally influence the samples' pore size. The samples A-MEOA-500 and A-TEOA-500 possessed pore sizes of around 4 nm regardless of the base used during the syntheses. In sample A-DEOA-500, however, the pore size lowered from 5.3 nm to 3.8 nm when the pH was adjusted to a higher value during the synthesis. In comparison, Sun et al. [11] and Wang et al. [14] synthesized mesoporous Al_2O_3 with a significant wider pore size distribution, over 20 nm and over 80 nm. Zhang et al., who synthesized Al_2O_3 through thermal treatment of crystalline $NH_4Al(OH)_2CO_3$, prepared from $NH_4Al(SO_4)_2$, reported about S_{BET} of synthesized materials became higher as the pH of the reaction mixture increased [13].

3.3. Properties of the materials synthesized from triethanolamine at pH = 7.5 after thermal treatment at different temperatures

The XRD patterns of the A-TEOA-7.5-T samples are shown in Fig. 7. The patterns of samples A-TEOA-7.5-500, A-TEOA-7.5-600, A-TEOA-7.5-700 and A-TEOA-7.5-900 show broad peaks at 19.8°, 31.8°, 37.3°, 39.6°, 45.9°, 60.6° and 66.7° 2θ, which are consistent with γ-Al_2O_3 (PDF card 01-079-1558). On closer inspection of the diffraction peaks in the low-angle part of the XRD patterns in the range between 10° and 40° 2θ (see inset in Fig. 7), also less intensive diffractive peaks could be observed, although they are broad. Increasing the temperature of the thermal treatment from 500 °C to 900 °C led to visibly narrower (but still very broad) peaks, confirming an increasing crystallographic order with increasing temperature, but the crystallinity remained low even at 900 °C, as is usually observed for this phase. Zhang et al. reported that their samples transformed from amorphous to crystalline phase γ-Al_2O_3 at 700 °C, with the crystallinity increasing up to 1000 °C when they started to transform to α-Al_2O_3 and θ-Al_2O_3 [13].

The XRD pattern of sample A-TEOA-7.5-1300 showed strong peaks at 25.5°, 35.1°, 37.6°, 43.5°, 52.5°, 57.6°, 66.6°, 68.1° and 76.8° 2θ, in addition to many weaker peaks, belonging to corundum (α-Al_2O_3, PDF card 01-075-1862).

FTIR spectra of the A-TEOA-7.5-T samples are presented in Fig. 8. With the exception of the sample A -TEOA-7.5-1300, the spectra of all the samples showed bands at the same wave numbers, as shown in Fig. 5. Bands in the FTIR spectra of the samples A-TEOA-7.5-500, A-TEOA-7.5-

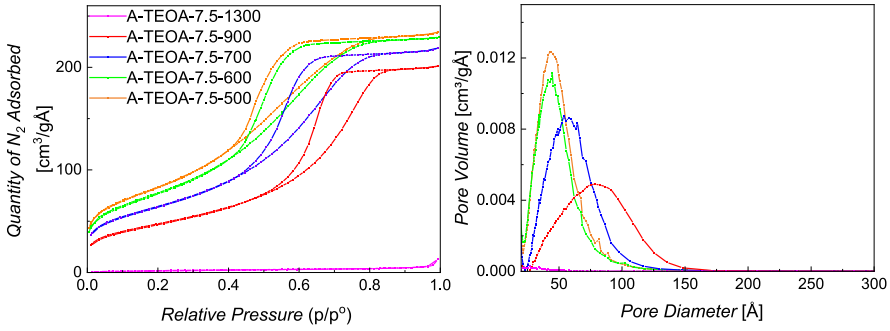

Fig. 9. Nitrogen adsorption–desorption isotherms (left) and BJH pore size distribution (right) of the A-TEOA-7.5-T samples.

Table 3
Specific surface, pore volume and pore diameter of the A-TEOA-7.5-T samples.

Sample name	S_{BET} (m^2/g)	V_p (cm^3/g)	D_p (nm)
A-TEOA-7.5-500	302	0.36	4.4
A-TEOA-7.5-600	281	0.35	4.5
A-TEOA-7.5-700	232	0.37	5.9
A-TEOA-7.5-900	171	0.36	7.9
A-TEOA-7.5-1300	7	0.01	/

600, A-TEOA-7.5-700 and A-TEOA-7,5–900 were assigned at 3466 cm^{-1}, 2037 cm^{-1}, 1640 cm^{-1}, 837 cm^{-1} and 563 cm^{-1}. The FTIR spectrum of sample A (TEOA-7.5-1300) showed two bands, at 566 cm^{-1} and 768 cm^{-1}, which both belong to bending and twisting vibrations for Al-O [16]. The absence of the bands at 3466 cm^{-1} and 1640 cm^{-1}, which correspond to O-H stretching and bending vibrations [16], in the spectrum of the A-TEOA-7.5-1300 sample indicates an absence of the OH groups. We propose that the OH groups present in γ-Al_2O_3 were no longer present in α-Al_2O_3.

The nitrogen adsorption–desorption isotherms and BJH pore size distribution curves of the A-TEOA-7.5-T samples are presented in Fig. 9. With the exception of the isotherm for the A-TEOA-7.5-1300 sample, all the isotherms correspond to type IV, as with the A-TEOA-500 samples (Fig. 6), confirming a mesoporous structure, which indicates the mesoporosity of the samples. We confirmed the mesoporous structure was maintained in the samples up to a thermal treatment temperature of 900 °C. In contrast, the isotherm of the A-TEOA-7.5-1300 sample corresponds to a type III isotherm and indicates the formation of non-porous material. The pore size distribution is broader and the pore size larger in the samples thermally treated at higher temperatures. The specific surface, pore volume and pore diameter of the samples are presented in Table 3.

The specific surface, pore volume and pore diameter of the A-TEOA-T samples are presented in Table 3. The specific surface area of the samples (Table 3) decreased as the temperature of the thermal treatment increased in the A-TEOA-T samples, exhibiting values between 302 m^2/g and 7 m^2/g. Byun et al. achieved significantly lower surface areas (all below 200 m^2/g) at similar calcination temperatures [4]. With the exception of A-TEOA-7.5-1300, the pore volume was similar in all of the samples, with a value of approximately 0.36 cm^3/g (Table 3). The A-TEOA-7.5-1300 sample was non-porous, as already described (Fig. 9); the porosity could therefore not be evaluated, but the pore volume was approximately 0.01 cm^3/g. The pore diameter of the samples thermally treated at higher temperatures increased from 4.4 to 7.9 nm. According to the XRD patterns and the nitrogen sorption results (Figs. 7 and 9), we propose that increased crystallization and thermal treatment at higher temperatures decrease the specific surface area, while the pores between the crystals become larger.

The TEM micrographs and experimental SAED (selected area electron diffraction) patterns of the A-TEOA-7.5-T samples, with added simulated patterns for the γ-Al_2O_3 and α-Al_2O_3 phases of the samples, are presented in Fig. 10. The γ-Al_2O_3 phase was simulated from ICSD 249140, Fd3-mZ using crystallite sizes of 2.5 and 10 nm and the α-Al_2O_3 phase from ICSD 10426, R3-cH with a crystallite size of 15 nm. The TEM micrograph for the A-TEOA-7.5-500 sample (Fig. 10a) confirmed the presence of mesoporous material, with the darker parts representing the material and the lighter parts representing the mesopores. We confirmed that the mesoporous structure consisted of nanoparticles with voids between them. Additionally, in the inset of Fig. 10a, the crystal planes in the nanoparticle can be confirmed, suggesting that the mesoporous structure consisted of nanocrystallites with pores between them. The estimated size of the crystals in the A-TEOA-7.5-500 sample was 2.5 nm. According to the SAED pattern (Fig. 10a—right), the presence of γ-Al_2O_3 could be confirmed in these samples by the presence of the crystal planes (311), (400) and (440). The micrograph of the A-TEOA-7.5-700 sample

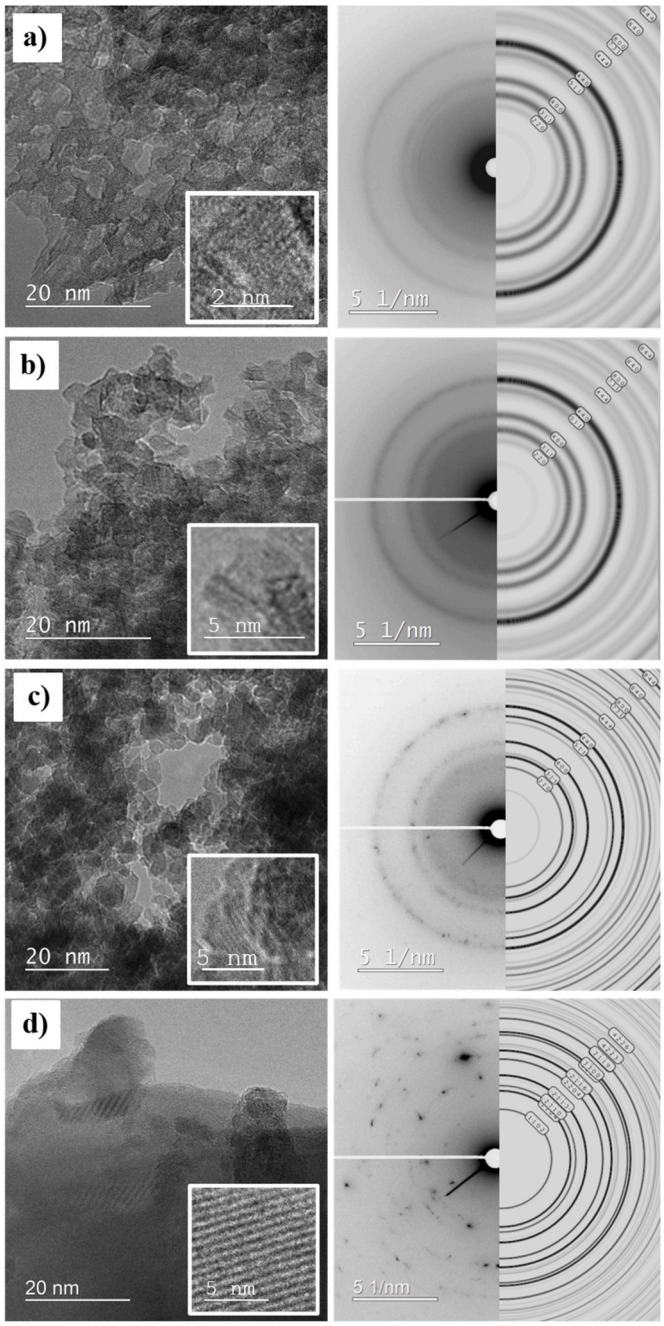

Fig. 10. TEM pictures (left) and experimental SAED patterns (right) with simulated γ-Al_2O_3 diffraction patterns: a) A-TEOA-7.5-500 with simulated γ-Al_2O_3 diffraction pattern using a crystallite size of 2.5 nm, b) A-TEOA-7.5-700 with simulated γ-Al_2O_3 diffraction pattern using a crystallite size of 2.5 nm, c) A-TEOA-7.5-900 with simulated γ-Al_2O_3 diffraction pattern using a crystallite size of 10 nm, d) A-TEOA-7.5-1300 with simulated α-Al_2O_3 diffraction pattern using a crystallite size of 150 nm. Insets represent the images at higher magnifications.

(Fig. 10b) shows less-defined mesoporous material with the presence of more particles (darker parts) and less pores (lighter parts). The size of the particles was estimated to be between 3 and 6 nm. The diffraction pattern of the A-TEOA-7.5-700 sample (Fig. 10b—right) also confirmed the presence of crystal planes of γ-Al_2O_3 at (311), (400) and (440). The micrograph of the A-TEOA-7.5-900 sample (Fig. 10c) shows mostly nanoparticles (dark parts) sized 5–9 nm and below, with larger pores (light part) between them. Crystal planes were also observed in the micrograph of these samples (inset in Fig. 10c), confirming γ-Al_2O_3 with

the presence of (311), (400) and (440) planes (Fig. 10c—right). In the micrograph of the A-TEOA-7.5-1300 sample (Fig. 10d), mainly non-porous material could be observed (mainly dark parts are observed), with particles of 400 nm in size. The SAED pattern (Fig. 10d—right) showed the presence of crystal planes at (1102), (110), (2110), (2116) and (3300), confirming the presence of α-Al_2O_3. The confirmed presence of the crystal planes (311), (400) and (440) matched the crystal planes in the simulated diffraction pattern of γ-Al_2O_3 from card ICSD 249140; we therefore propose that the γ-Al_2O_3 phase is present in the A-TEOA-7.5-500, A-TEOA-7.5-700 and A-TEOA-7.5-900 samples. In the A-TEOA-7.5-1300 sample (Fig. 10d—right), the crystal planes match the simulated diffraction pattern of α-Al_2O_3 from card ICSD 10426; we therefore propose that α-Al_2O_3 was present in the A-TEOA-7.5-1300 sample. We found that the samples that had undergone temperature treatment up to 900 °C were all γ-Al_2O_3, whereas the size of the crystallites was different—with a rise in the temperature of the thermal treatment the size of the crystals increased and the pore size decreased. According to the XRD patterns (Fig. 4), we propose that the materials A-MEOA-500, A-DEOA-500 and A-TEOA-500 are in partly crystalline phases with additional amorphous parts.

4. Conclusion

In this study, mesoporous γ-Al_2O_3materials were successfully synthesized using the hydrothermal pH-adjusted method, using ethanolamines (monoethanolamine, diethanolamine and triethanolamine) as the key synthesis variables. The findings revealed that the type of ethanolamine, the pH adjustment and thermal treatment significantly influenced the textural and structural properties of the synthesized materials. Prior to thermal treatment, γ-AlO(OH) was present in all samples, while triethanolamine hydrochloride formed in the samples synthesized with triethanolamine. Thermal treatment at 500 °C yielded mesoporous γ-Al_2O_3, with pores located between nanocrystals. The materials synthesized with triethanolamine exhibited a narrower pore size distribution and a higher specific surface area, with the highest values observed when the pH adjustment was higher. Nitrogen physisorption demonstrated that the pore size, specific surface area and pore volume were strongly influenced by both the synthesis parameters and the thermal treatment. For the samples prepared with ethanolamine and diethanolamine, the pH adjustment affected the pore volume but not the pore diameter, whereas the triethanolamine-based materials exhibited stable pore volumes across varying pH values. The thermal treatment temperature had a great impact, with pore diameters increasing significantly between 500 °C and 900 °C, while the specific surface areas decreased, due to enhanced crystallinity and phase transitions. By 1300 °C, all materials had transformed into non-porous α-Al_2O_3. TEM micrographs confirmed that mesopores were formed between the γ-Al_2O_3 crystals, with higher thermal treatment temperatures resulting in larger crystal sizes and correspondingly larger pores. The results highlight the crucial role of synthesis parameters and thermal treatment in tailoring mesoporous materials. Among the factors studied, the thermal treatment temperature was the most influential in controlling the pore diameter, specific surface area and phase stability. This work demonstrates the versatility of the hydrothermal method in producing mesoporous alumina with the stability of mesopores up to 900 °C, and the ability to adjust the pore diameters through thermal treatment makes these materials highly promising for different applications.

CRediT authorship contribution statement

Klara Šparlek: Writing – original draft, Investigation, Conceptualization. **Romana Cerc Korošec:** Writing – review & editing, Writing – original draft, Investigation. **Goran Dražić:** Writing – review & editing, Investigation. **Anton Meden:** Writing – review & editing, Writing – original draft, Supervision, Investigation, Conceptualization. **Erika Švara Fabjan:** Writing – review & editing, Writing – original draft, Supervision, Investigation, Conceptualization.

Declaration of competing interest

The authors declare that they have no known competing financial interests or personal relationships that could have appeared to influence the work reported in this paper.

Acknowledgments

We acknowledge the financial support from the Slovenian Research and Innovation Agency through the core research programs No. P2-0273, P1-0175, P1-0134, P2-0421 and P2-0393. We are grateful to Catherine Earles for proofreading the English manuscript.

Appendix A. Supplementary data

Supplementary data to this article can be found online at https://doi.org/10.1016/j.ceramint.2025.05.353.

References

[1] Q. Meng, C. Liu, X. Yu, Q. Zhu, X. Kong, Construction of bimetallic CuMn catalysts supported on ordered mesoporous Al2O3-CeO2 for high-efficient synthesis of furfuryl alcohol from furfural, J. Alloys Compd. 1008 (2024) 176499, https://doi.org/10.1016/j.jallcom.2024.176499.
[2] N.M. Stuart, K. Sohlberg, The microstructure of γ-Alumina, Energies 14 (2021) 6472, https://doi.org/10.3390/en14206472.
[3] K.S.W. Sing, D.H. Everett, R.A.W. Haul, L. Moscou, R.A. Pierotti, J. Rouquerol, T. Siemieniewska, Reporting physisorption data for gas/solid systems with special reference to the determination of surface area and porosity, Pure Appl. Chem. 57 (1985) 603–619, https://doi.org/10.1515/pac-2014-1117.
[4] M.Y. Byun, J.S. Kim, D.-W. Park, M.S. Lee, Influence of calcination temperature on the structure and properties of Al2O3 as support for Pd catalyst, Kor. J. Chem. Eng. 35 (2018) 1083–1088, https://doi.org/10.1007/s11814-018-0015-y.
[5] X. Xu, S.K. Megarajan, Y. Zhang, H. Jiang, Ordered mesoporous alumina and their composites based on evaporation induced self-assembly for adsorption and catalysis, Chem. Mater. 32 (2020) 3–26, https://doi.org/10.1021/acs.chemmater.9b03873.
[6] G. Zhang, K. Zhao, Q. Zhu, X. Kong, Design of n-doped carbon materials assisted Co CoOx anchoring on mesoporous Silica spheres, ChemCatChem 14 (2022), https://doi.org/10.1002/cctc.202201001.
[7] L. Ma, G. Zhang, Y. Dong, S. Dou, Q. Meng, P. Yan, L. Liu, X. Kong, Hydrodeoxygenation of lignin derivatives over Ni-Re bimetallic catalyst supported on mesoporous carbon sphere, J. Environ. Chem. Eng. 11 (4) (2023), https://doi.org/10.1016/j.jece.2023.110215.
[8] J.-L. Blin, F. Jonas, L. Michelin, S. Rigolet, L. Josien, L. Vidal, L. Richaudeau, B. Lebeau, Insights into formation and properties of amorphous mesostructured alumina, Microporous Mesoporous Mater. 367 (2024) 112997, https://doi.org/10.1016/j.micromeso.2024.112997.
[9] M.M. Amini, M. Mirzaee, Effect of solution chemistry on preparation of boehmite by hydrothermal assisted sol-gel processing of aluminum alkoxides, J. Sol. Gel Sci. Technol. 36 (2005) 19–23, https://doi.org/10.1007/s10971-005-4790-7.
[10] P.F. Fulvio, R.I. Brosey, M. Jaroniec, Synthesis of mesoporous alumina from boehmite in the presence of triblock copolymer, ACS Appl. Mater. Interfaces 2 (2010) 588–593, https://doi.org/10.1021/am9009023.
[11] Z.-X. Sun, T.-T. Zheng, Q.-B. Bo, M. Du, W. Forsling, Effects of calcination temperature on the pore size and wall crystalline structure of mesoporous alumina, J. Colloid Interface Sci. 319 (2008) 247–251, https://doi.org/10.1016/j.jcis.2007.11.023.
[12] G.L. Teoh, K.Y. Liew, W.A.K. Mahmood, Synthesis and characterization of sol–gel alumina nanofibers, J. Sol. Gel Sci. Technol. 44 (2007) 177–186, https://doi.org/10.1007/s10971-007-1631-x.
[13] L. Zhang, Y. Wu, L. Zhang, Y. Wang, M. Li, Synthesis and characterization of mesoporous alumina with high specific area via coprecipitation method, Vacuum 133 (2016) 1–6, https://doi.org/10.1016/j.vacuum.2016.08.005.
[14] W. Wang, K. Zhang, Y. Yang, H. Liu, Z. Qiao, H. Luo, Synthesis of mesoporous Al2O3 with large surface area and large pore diameter by improved precipitation method, Microporous Mesoporous Mater. 193 (2014) 47–53, https://doi.org/10.1016/j.micromeso.2014.03.008.
[15] S.-F. Wang, X. Xiang, G. Sun, X.-L. Gao, B. Chen, Q.-P. Ding, Z.-J. Li, C. Zhang, X.-T. Zu, Role of pH, organic additive, and chelating agent in gel synthesis and fluorescent properties of porous monolithic alumina, J. Phys. Chem. C 117 (2013) 5067–5074, https://doi.org/10.1021/jp311055b.
[16] A. Amirsalari, S. Farjami Shayesteh, Effects of pH and calcination temperature on structural and optical properties of alumina nanoparticles, Superlattice. Microst. 82 (2015) 507–524, https://doi.org/10.1016/j.spmi.2015.01.044.
[17] N. Xu, Z. Liu, Y. Dong, T. Hong, L. Dang, W. Li, Controllable synthesis of mesoporous alumina with large surface area for high and fast fluoride removal,

Ceram. Int. 42 (2016) 15253–15260, https://doi.org/10.1016/j.ceramint.2016.06.164.
[18] Q. Liu, A. Wang, X. Wang, T. Zhang, Morphologically controlled synthesis of mesoporous alumina, Microporous Mesoporous Mater. 100 (2007) 35–44, https://doi.org/10.1016/j.micromeso.2006.10.011.
[19] F. Gholizadeh, A. Izadbakhsh, J. Huang, Y. Zi-Feng, Catalytic performance of cubic ordered mesoporous alumina supported nickel catalysts in dry reforming of methane, Microporous Mesoporous Mater. 310 (2021) 110616, https://doi.org/10.1016/j.micromeso.2020.110616.
[20] S. Wu, Y. Han, Y.-C. Zou, J.-W. Song, L. Zhao, Y. Di, S.-Z. Liu, F.-S. Xiao, Synthesis of heteroatom substituted SBA-15 by the "pH-Adjusting" method, Chem. Mater. 16 (2004) 486–492, https://doi.org/10.1021/cm0343857.
[21] E. Choi, K. Song, S. An, K. Lee, M. Youn, K. Park, S. Jeong, H. Kim, Cu/ZnO/AlOOH catalyst for methanol synthesis through CO2 hydrogenation, Kor. J. Chem. Eng. 35 (2018) 73–81, https://doi.org/10.1007/s11814-017-0230-y.
[22] https://webbook.nist.gov/cgi/cbook.cgi?ID=C141435&Mask=200#Mass-Spec, (accessed 2 of July 2024).
[23] https://www.fishersci.at/shop/products/triethanolamine-hydrochloride-99-thermo-scientific-1/11407627, (accessed 2 of July 2024).
[24] A. Abdelkader, B.M. Hussien, E.M. Fawzy, A.A. Ibrahim, Boehmite nanopowder recovered from aluminum cans waste as a potential adsorbent for the treatment of oilfield produced water, Appl. Petrochem. Res. 11 (2021) 137–146, https://doi.org/10.1007/s13203-021-00267-x.
[25] P.P. Nampi, S. Ghosh, K.G. Warrier, Calcination and associated structural modifications in boehmite and their influence on high temperature densification of alumina, Ceram. Int. 37 (2011) 3329–3334, https://doi.org/10.1016/j.ceramint.2011.04.129.